PNAS RESEARCH ARTICLE | NEUROSCIENCE OPEN ACCESS

Inactivation of microglial LXRβ in early postnatal mice impairs microglia homeostasis and causes long-lasting cognitive dysfunction

Keyi Lv[a], Yi Luo[a], Tianyao Liu[a], Meiling Xia[a], Hong Gong[a], Dandan Zhang[a], Xuan Chen[b], Xin Jiang[a], Yulong Liu[a], Jiayin Liu[a], Yulong Cai[a], Per Antonson[c], Margaret Warner[d], Haiwei Xu[b,1], Jan-Åke Gustafsson[c,d,1], and Xiaotang Fan[a,1]

Affiliations are included on p. 10.

Contributed by Jan-Åke Gustafsson; received May 30, 2024; accepted February 28, 2025; reviewed by George P. Chrousos and Bo Peng

Microglia, the largest population of brain immune cells, play an essential role in regulating neuroinflammation by removing foreign materials and debris and in cognition by pruning synapses. Since liver X receptor β (LXRβ) has been identified as a regulator of microglial homeostasis, this study examined whether its removal from microglia affects neuroinflammation and cognitive function. We used a cell-specific tamoxifen-inducible Cre-loxP-mediated recombination to remove LXRβ from microglia specifically. We now report that ablation of LXRβ in microglia in early postnatal life led to a reduction in microglial numbers, distinct morphological changes indicative of microglial activation, and enhanced synapse engulfment accompanied by cognitive deficits. Removal of LXRβ from microglia in adult mice caused no cognitive defects. RNAseq analysis of microglia revealed that loss of LXRβ led to reduced expression of SAll1, a master regulator of microglial homeostasis, while increasing expression of genes associated with microglial activation and CNS disease. This study demonstrates distinctly different functions of microglial LXRβ in developing and adult mice and points to long-term consequences of defective LXRβ signaling in microglia in early life.

LXRβ | microglia | cognitive function | microglia homeostasis | synapse engulfment

Significance

Microglia control neuroinflammation by eliminating foreign substances and debris and pruning synapses that affect cognitive function. Our study reveals that early ablation of LXRβ in the postnatal microglia results in a decrease in microglial numbers and changes in their morphology, which suggests that microglial activation has occurred. Furthermore, removing microglial LXRβ in mice during the neonatal period, but not at P30, heightened synapse engulfment and resulted in cognitive impairments. These findings show that the early deletion of LXRβ in postnatal microglia can cause dysregulation of microglial functions, including inflammation, synaptic pruning, and cognitive function.

Microglia, resident macrophages of the central nervous system (CNS), are crucial for maintaining CNS homeostasis, immune functions, synaptic plasticity, and synaptic function (1). During brain development, microglia interact with other cell types in the CNS to support crucial processes that shape synaptic organization and contribute to higher cognitive functions (2). Previous studies have demonstrated that a peripheral inflammatory challenge can affect the hippocampus and trigger excessive microglial activation, leading to memory impairments (3, 4). Additionally, cognitive dysfunction following brain injury has been linked to activation of microglia (5–8). Synaptic loss is a significant issue in cognitive impairment. Several lines of evidence indicate that abnormal microglia may be responsible for the aberrant elimination of synapses, leading to cognitive and emotional dysfunction (9–11). In 2021, Ding et al. demonstrated that deleting the microglial signal regulatory protein (SIRPα) led to increased phagocytosis, synaptic loss, and exacerbated cognitive impairment (12). Recent advances in single-cell RNA sequencing (scRNA-seq) have revealed that there are not just two states but multiple states of microglia (13). The transition of microglia from homeostatic to reactive status profoundly alters the microglial transcriptome, leading to morphological changes, increased phagocytic activity, expression of various immune receptors, and enhanced cytokine secretion (14).

Liver X receptors (LXRs) are members of the nuclear receptor superfamily, which includes LXRα and LXRβ. LXRα is mainly found in peripheral organs involved in lipid metabolism, while LXRβ is abundantly expressed in the brain and contributes to multiple physiological and pathological processes (15–19). Because of its widespread expression in brain cells, deletion of LXRβ from the mouse genome has different effects from deletion in individual brain cells. A complete deletion of the LXRβ in mice caused abnormalities in progenitor cells and granule cells in the dentate gyrus (DG), resulting in behaviors similar to those observed in autism spectrum disorder (17), loss of dopaminergic neurons in the substantia nigra (20), and loss of large motor neurons in the ventral horn of the spinal cord (21). In contrast, specific deletion of LXRβ in astrocytes triggered changes in spontaneous excitatory synaptic transmission in the medial prefrontal cortex and led to anxiety-like behavior (22). Several studies have demonstrated that LXRβ has a profound inhibitory impact on microglial activation (23, 24). LXR agonists have been shown to effectively decrease the production of proinflammatory mediators, such as NO, IL-1β,

Author contributions: H.X., J.-Å.G., and X.F. designed research; K.L., Y. Luo, T.L., M.X., H.G., D.Z., X.C., X.J., Y. Liu, J.L., and Y.C. performed research; P.A. contributed new reagents/analytic tools; K.L., Y. Luo, T.L., H.X., and X.F. analyzed data; and K.L., M.W., H.X., J.-Å.G., and X.F. wrote the paper.

Reviewers: G.P.C., Ethniko kai Kapodistriako Panepistemio Athenon; and B.P., Fudan University.

The authors declare no competing interest.

[1]To whom correspondence may be addressed. Email: haiweixu2001@163.com, jgustafsson@uh.edu, or fanxiaotang2005@163.com.

This article contains supporting information online at https://www.pnas.org/lookup/suppl/doi:10.1073/pnas.2410698122/-/DCSupplemental.

Published April 10, 2025.

and IL-6, in microglia and astrocytes, thereby mitigating microglial inflammation (25–29). Furthermore, cognitive and emotional dysfunction caused by lipopolysaccharide injection or chronic unpredictable mild stress was prevented by LXR agonists. This was accompanied by the suppression of microglial M1-polarization and restoration of synaptic plasticity in the hippocampus (30). In a study involving primary microglia cultures, LXRβ was identified as one of the transcription factors that suppress proinflammatory disease-associated microglia (DAM) responses and suppress homeostatic and anti-inflammatory responses (31).

In the study presented here, we created a conditional knockout of LXRβ, specifically targeting microglia. We found that loss of microglial expression of LXRβ in the first 2 wk of postnatal life impeded the development and maturation of microglia and cognitive dysfunction associated with a loss of synapses. These changes were accompanied by transcriptional changes related to a shift from microglial homeostasis to DAM states in the hippocampus and cerebral cortex. Removal of LXRβ in microglia in adulthood did not affect cognitive function.

Results

Creation of Microglial-Specific LXRβ Knockout Mice. To investigate the role of LXRβ in microglia, we generated conditional LXRβ knockout mice using Cx3cr1^{CreER} mice (Fig. 1*A*). We confirmed the deletion of LXRβ in microglia using PCR of genomic DNA (Fig. 1*B*). After administration of tamoxifen, the level of LXRβ mRNA in microglia from microglial-specific LXRβ KO(cKO) at P14 was markedly reduced compared with LXRβ$^{fl/fl}$ mice which are used as controls in this study (Fig. 1*C*). Immunostaining for the microglial marker, Iba1, revealed that virtually all GFP$^+$ cells were Iba1$^+$ in the hippocampus and cortex of the Cx3cr1^{CreER} mice after tamoxifen treatment (Fig. 1*D*). To confirm the specificity of Cre recombination of Cx3cr1^{CreER} mice, Cx3cr1^{CreER} mice were crossed with Rosa-tdTomato mice (*SI Appendix*, Fig. S1*A*), and the tdTomato-positive cells in the hippocampus and cortex were characterized. Most of the tdTomato-positive cells were coimmunostained with the microglia marker, Iba1 (Fig. 1*E*), while very few tdTomato-positive cells costained with NeuN (neuronal marker), S100β (astrocyte marker), or Olig2 (oligodendrocytic marker) (*SI Appendix*, Fig. S1 *B–D*). These results demonstrate that Cre-mediated recombination did ablate LXRβ expression in microglia in an inducible manner in Cx3cr1^{CreER}:LXRβ$^{fl/fl}$ mice (cKO mice) specifically and efficiently. Quantification of CD11b$^+$CD45^{low} brain microglia using flow cytometry showed microglia-specific ablation of LXRβ caused a reduction of total microglia in the brain following tamoxifen administration without alterations in lymphocyte or macrophage populations at P14 (Fig. 1 *F* and *G*). We observed no significant alteration in the percentages of F4/80$^+$/Ly6C$^+$ myeloid cells in the brain of these mice, indicating that there were no infiltrating inflammatory monocyte-derived cells (*SI Appendix*, Fig. S2). Cx3cr1 expression in peripheral monocytes and inflammatory macrophages of Cx3cr1^{CreER} mice has been reported, and we found no significant difference in the percentages of myeloid populations in blood and spleen between cKO and control mice at P14 (*SI Appendix*, Fig. S3).

Microglia-Specific Ablation of LXRβ in Early Postnatal Life Results in Decreased Microglia Density in the Hippocampus and Cortex. We confirmed a profound decrease in the density of Iba1$^+$ cells in the CA1, CA3, and dentate gyrus (DG) of the hippocampus and cerebral cortex in microglial-specific KO mice at P7 (Fig. 1 *H* and *I*). Pu.1, a master transcriptional regulator of microglial development (32), is required for LXR and TLR-dependent gene expression (31). In Cx3cr1^{CreER}:LXRβ$^{fl/fl}$ mutant mice at P7, the number of Pu.1$^+$ cells was markedly reduced (Fig. 1 *H* and *J*).

Specific Ablation of LXRβ in Microglia Results in the Transformation to Activated Status. Using Iba1 immunostaining, we assessed the effects of LXRβ deletion in microglia on microglia at P14 and P30. The staining showed that, compared to controls, there was a significant reduction in microglial cell density in the hippocampus and cerebral cortex in male cKO mice at P14 (Fig. 2 *A* and *C*). The decrease in microglia density in the hippocampus and cerebral cortex was transient and returned to normal levels at P30 (Fig. 2*D*). To analyze the role of LXRβ on the reduction in microglia, we examined the expression of Ki67 in Iba1$^+$ cells. There was a significant reduction in the numbers and percentage of proliferating microglia (Ki67$^+$/Iba1$^+$) in cKO mice compared to control mice at P7 and P14. However, by P30, there were few proliferating microglia in either genotype (*SI Appendix*, Fig. S4). Thus, there is a crucial role of LXRβ in the proliferation of microglia in early postnatal life. The marked difference in morphology between homeostatic and activated microglia has been described (33). Microglia in the cKO mice at P14 were activated, as evidenced by shorter, stubbier processes and a larger soma size compared to microglia in control mice (Fig. 2*B*). Semiautomatic quantitative morphometric 3D measurements of microglia confirmed a significantly reduced branch length (Fig. 2 *E* and *G*), number of branches (*SI Appendix*, Fig. S5 *B* and *E*), number of junctions (*SI Appendix*, Fig. S5 *C* and *F*), and an increase in soma area(Fig. 2 *F* and *H*) in the hippocampus and cerebral cortex in P14 and P30 male cKO mice. As shown in Fig. 2 *A* and *B*, microglia in P30 cKO mice showed some morphological alterations, but the phenotype is not as prominent as that observed at P14.

Analysis of microglia from cKO and control P14 mice, sorted by flow cytometry, revealed a higher ratio of CD86$^+$ (Fig. 2*I*) and major histocompatibility complex class II (MHC-II) (Fig. 2*J*) in the cKO microglia indicating increased activation profile. qRT-PCR analysis of FACS-sorted CD11b$^+$CD45^{low} confirmed that there was an increase in the mRNA of inflammatory cytokines TNFα, IL-1β, and IL-6, and higher expression of the microglia activation genes MHC-II, CD68, and ApoE in the cKO mice (Fig. 2*K*). Consistent with these results, we found that LXRβ ablation in microglia upregulated mRNA expression of proinflammatory cytokines TNFα, IL-6, IL-1β at P14 (*SI Appendix*, Fig. S5*A*) and P30 (*SI Appendix*, Fig. S5*D*) in the hippocampus and cerebral cortex. Taken together, these data show that in microglial-specific KO mice, more activated microglia in the hippocampus and cerebral cortex both at P14 and P30.

Specific Ablation of LXRβ in Microglia Shows Altered Transcriptional Signatures of Microglia at P14. Upon RNA-seq analysis of isolated microglia from P14 cKO and control mice (Fig. 3*A*), hierarchical clustering showed clear segregation of the genes that were differentially expressed between the microglia-ablated LXRβ and controls (Fig. 3*B*). Gene ontology (GO) analysis showed significant enrichment of biological processes including regulation of inflammatory response, regulation of tumor necrosis factor production, morphogenesis of a branching structure, regulation of axonogenesis, axon extension, and neuroinflammatory response. In the molecular function category, genes were enriched in clusters, including immune receptor activity, cytokine receptor activity, chemokine receptor activity, purinergic nucleotide receptor activity, and nucleotide receptor activity (Fig. 3*C*). Transcriptome

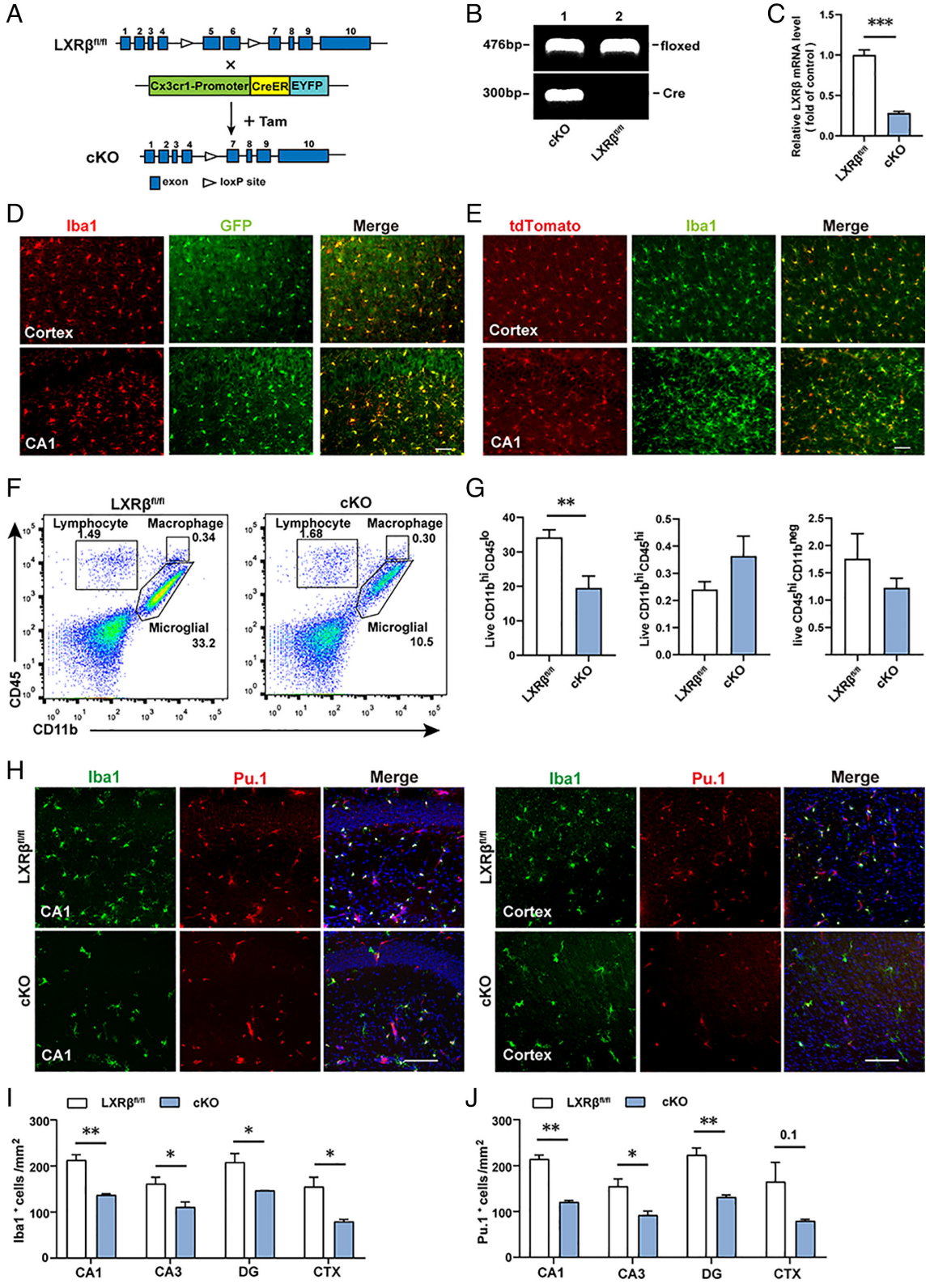

Fig. 1. Generation of microglial LXRβ conditional knockout mice. (*A*) Schematic diagram of constructing microglial LXRβ conditional knockout mice from breeding Cx3cr1-Cre mice with mice carrying homozygous LXRβ-floxed allele. (*B*) PCR analysis of genomic DNA for Genotyping of the mice. (*C*) Microglia isolation from LXRβ$^{fl/fl}$ and cKO mice for LXRβ mRNA analysis (N = 4 to 5 mice in each group). (*D*) Representative images depicting GFP coimmunofluorescence with microglia marker Iba1 in the cortex and hippocampus CA1 from microglia-specific Cre expression in the Cx3cr1$^{CreER/+}$ mouse following tamoxifen injection. (Scale bar, 20 μm.) (*E*) Representative images depicting Iba1 with tdTomato in the hippocampus CA1 and cortex in Cx3cr1$^{CreER/+}$; Ai9 mouse following tamoxifen injection. (Scale bar, 20 μm.) (*F*) Flow cytometric analysis of the whole brain from LXRβ$^{fl/fl}$ and cKO mice at P14 was performed to determine percentages of microglia, macrophages, and lymphocyte populations within live cells. (*G*) The quantitative percentages of microglia (CD45^{low} CD11b^{hi}), macrophages (CD45^{high} CD11b^{high}), and lymphocytes (CD45^{high} CD11b^{negative}) populations within live cells at P14 (N = 6 mice in each group). (*H*) Representative images depicting Iba1 with Pu.1 in the hippocampus CA1 and Cortex in LXRβ$^{fl/fl}$ and cKO mice at P7 following tamoxifen injection at P1 to P3. (Scale bar, 50 μm.) (*I*) The quantitative density of Iba1^{+} cells in hippocampus CA1, CA3, DG, and cortex at P7(N = 3 mice in each group). (*J*) The quantitative density of Pu.1^{+} cells in hippocampus CA1, CA3, DG, and cortex at P7(N = 3 mice in each group). Data are expressed as mean ± SEM. Student's *t* test, **P* < 0.05, ***P* < 0.01, ****P* < 0.001.

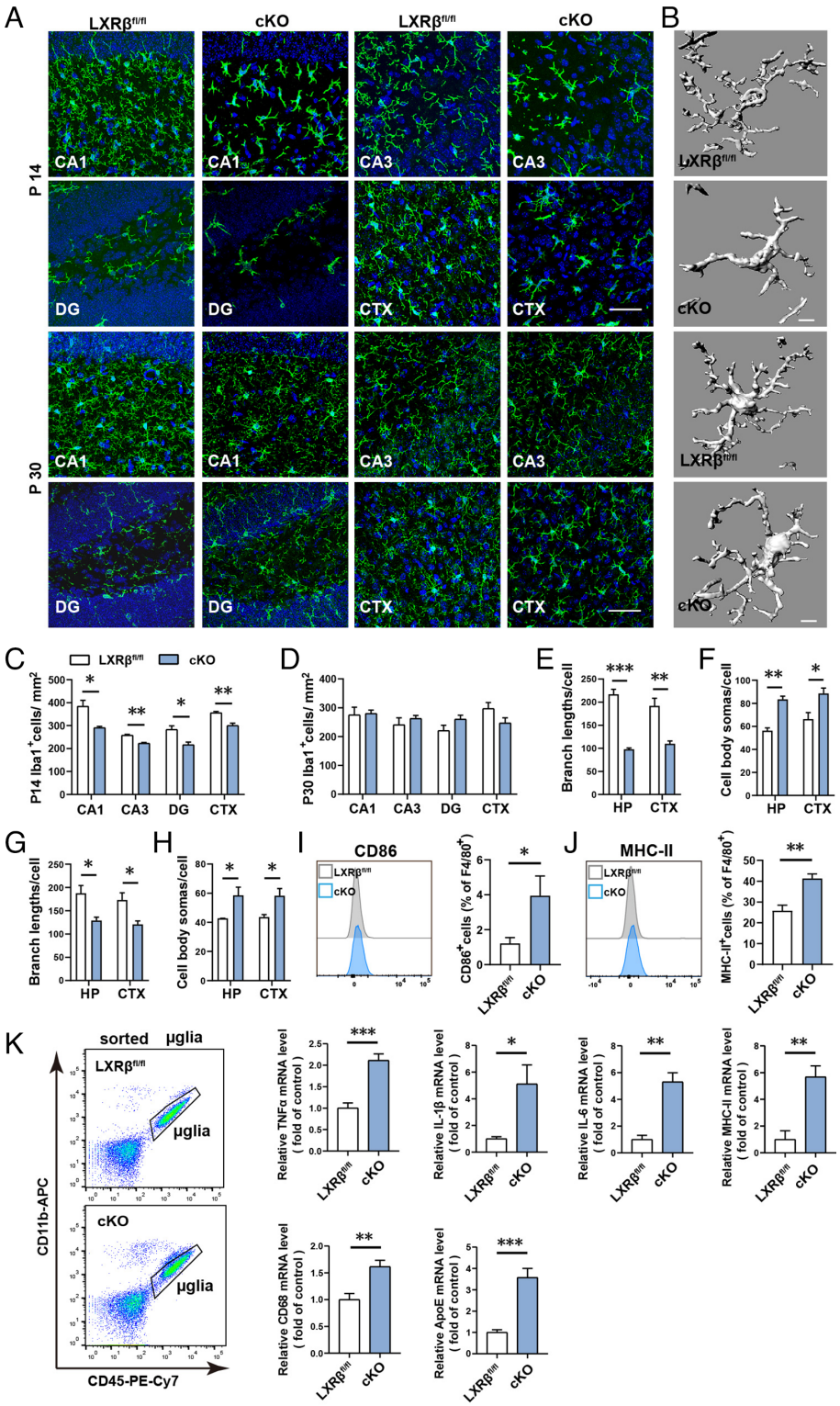

Fig. 2. Deletion of LXRβ in microglia affects microglia cell density, morphology, and activation in mice. (*A*) Representative images depicting microglia marker Iba1 in the hippocampal CA1, CA3, DG, and cortex (CTX) of LXRβ$^{fl/fl}$ and cKO mouse brains at P14 and P30. (Scale bar, 50 μm.) (*B*) Three-dimensional reconstruction in microglia of LXRβ$^{fl/fl}$ and cKO mouse at P14 and P30. (Scale bar, 5 μm.) (*C* and *D*) Microglia were counted as Iba1^{+}cells in the hippocampal CA1, CA3, DG, and CTX of LXRβ$^{fl/fl}$(N = 3) and cKO (N = 3) mouse brains at P14 (*C*) and P30 (*D*). (*E* and *F*) Quantitative analysis of branch lengths per cell (*E*) and cell body somas per cell (*F*) in the hippocampal CA1 and CTX of LXRβ$^{fl/fl}$ (N = 3) and cKO (N = 3) mice at P14. (*G* and *H*) Quantitative analysis of branch lengths per cell (*G*) and cell body somas per cell (*H*) in the hippocampal CA1 and CTX of LXRβ$^{fl/fl}$ (N = 3) and cKO (N = 3) mice at P30. (*I* and *J*) Flow cytometric analysis of the microglial from LXRβ$^{fl/fl}$ and cKO at postnatal 14 was performed to determine the percent of surface CD86 (*I*) and MHC-II (*J*) in F4/80^{+} (N = 4 to 5 mice per group). (*K*) Relative mRNA expression by qRT-PCR in the sorted microglia of LXRβ$^{fl/fl}$ and cKO mice at P14. (N = 3 to 4 mice per group). Data are expressed as mean ± SEM. Student's *t* test, *P < 0.05, **P < 0.01, ***P < 0.001.

data of LXRβ knockdown microglia were consistent with transcriptome data of P14 control microglia from published data (34, 35) (*SI Appendix*, Fig. S6). The heatmap diagram showed that P14 significantly downregulated genes were associated with microglia homeostasis in the microglia of the cKO mice. However, some genes linked to phagocytosis, cytokines, chemotaxis, and

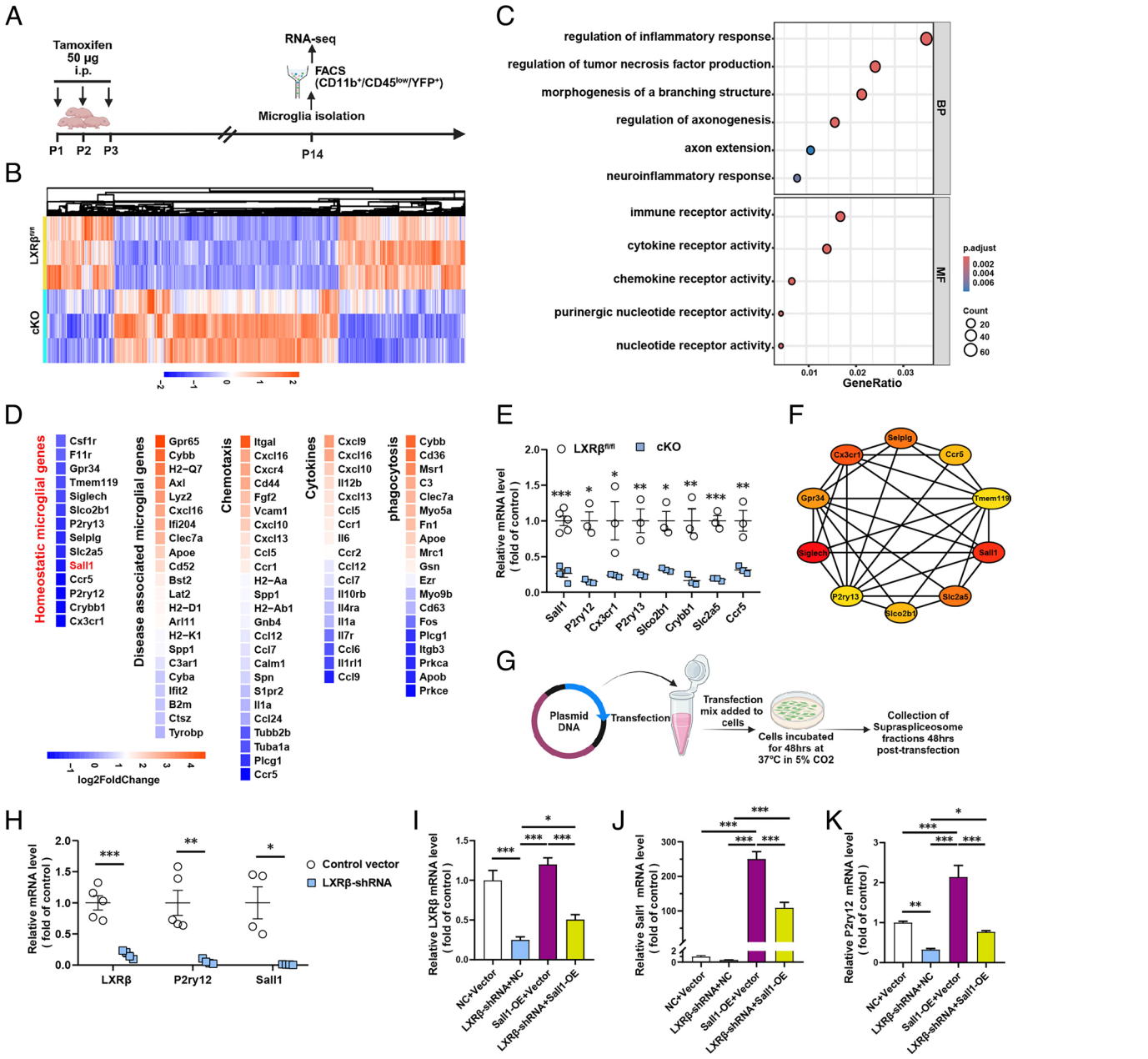

Fig. 3. Gene expression profiles in LXRβ deficiency in microglia. (*A*) Schematic diagram of RNA-Seq. (*B*) Heatmap shows hierarchical clustering of up-regulated (red) and down-regulated (blue) differentially expressed genes (DEGs) in microglia from deletion of LXRβ in microglia and LXRβ control analysis of RNA-Seq values (N = 3 mice per group). (*C*) Functional enriched GO pathways in biological processes and molecular function associated with homeostatic microglia genes. (*D*) Expression log2 (Fold change) of microglial-regulated genes clustered. (*E*) qRT-PCR was performed to evaluate the expression of homeostatic microglia genes in microglia sorted from $LXR\beta^{fl/fl}$ and cKO mice at P14 (N = 3 to 5 mice per group). (*F*) PPI analysis Sall1 interacts with homeostatic microglia genes. (*G*) Schematic diagram of plasmid transfection in BV2 cells. (*H–K*) qRT-PCR analysis of LXRβ, P2ry12, and Sall1 mRNA levels in the BV2 cell of control vector and LXRβ-shRNA (*H*) and qRT-PCR analysis of LXRβ (*I*), Sall1 (*J*), and P2ry12 (*K*) mRNA levels in the BV2 cell of NC+ vector, LXRβ-shRNA+NC, Sall1-OE+Vector, and LXRβ-shRNA+Sall1-OE (N = 3 to 5 per group). Data are expressed as mean ± SEM, $^{*}P < 0.05$, $^{**}P < 0.01$, or $^{***}P < 0.001$.

DAM were up-regulated in the cKO microglia (Fig. 3*D*). qRT-PCR confirmed a significant decrease in homeostatic microglial gene markers, including *Sall1*, *P2ry12*, *P2ry13*, *Cx3cr1*, *Crybb1*, *Slco2b1*, *Slc2a5*, and *Ccr5* (Fig. 3*E*), consistent changes with the RNA-Seq data. PPI analysis revealed that Sall1 could interact with microglial homeostasis genes (Fig. 3*F*). We used LXRβ-knockdown BV2 cells to investigate the potential role of Sall1 in restoring reduced P2ry12 expression (Fig. 3*G*). Consistent with the ablation of LXRβ in microglia in mice, LXRβ-knockdown in BV2 cells significantly decreased LXRβ, Sall1, and P2ry12 mRNA levels (Fig. 3*H*). Sall1 overexpression did not alter LXRβ mRNA level in BV2 cells, but rescued LXRβ mRNA level in LXRβ-shRNA treated BV2 cells (Fig. 3*I*). Sall1 overexpression significantly increased Sall1 mRNA level in BV2 cells, which could be inhibited by LXRβ-shRNA treatment (Fig. 3*J*). Notably, the decreased P2ry12mRNA levels in LXRβ-shRNA-treated BV2 cells could be rescued by Sall1 overexpression (Fig. 3*K*).

P2ry12 and Tmem119 Expression in LXRβ-Ablated Microglia. To assess how the absence of LXRβ in microglia influences the microglial homeostatic state, we examined the expression of two homeostatic microglia markers, P2ry12 and Tmem119, by immunohistochemistry. At P14, both P2ry12 (Fig. 4 *A* and *D*) and Tmem119 (Fig. 4 *B* and *E*) expression were significantly lower in the hippocampus and cerebral cortex of the cKO than in the controls. qRT-PCR analysis of the brains at P14 confirmed the loss

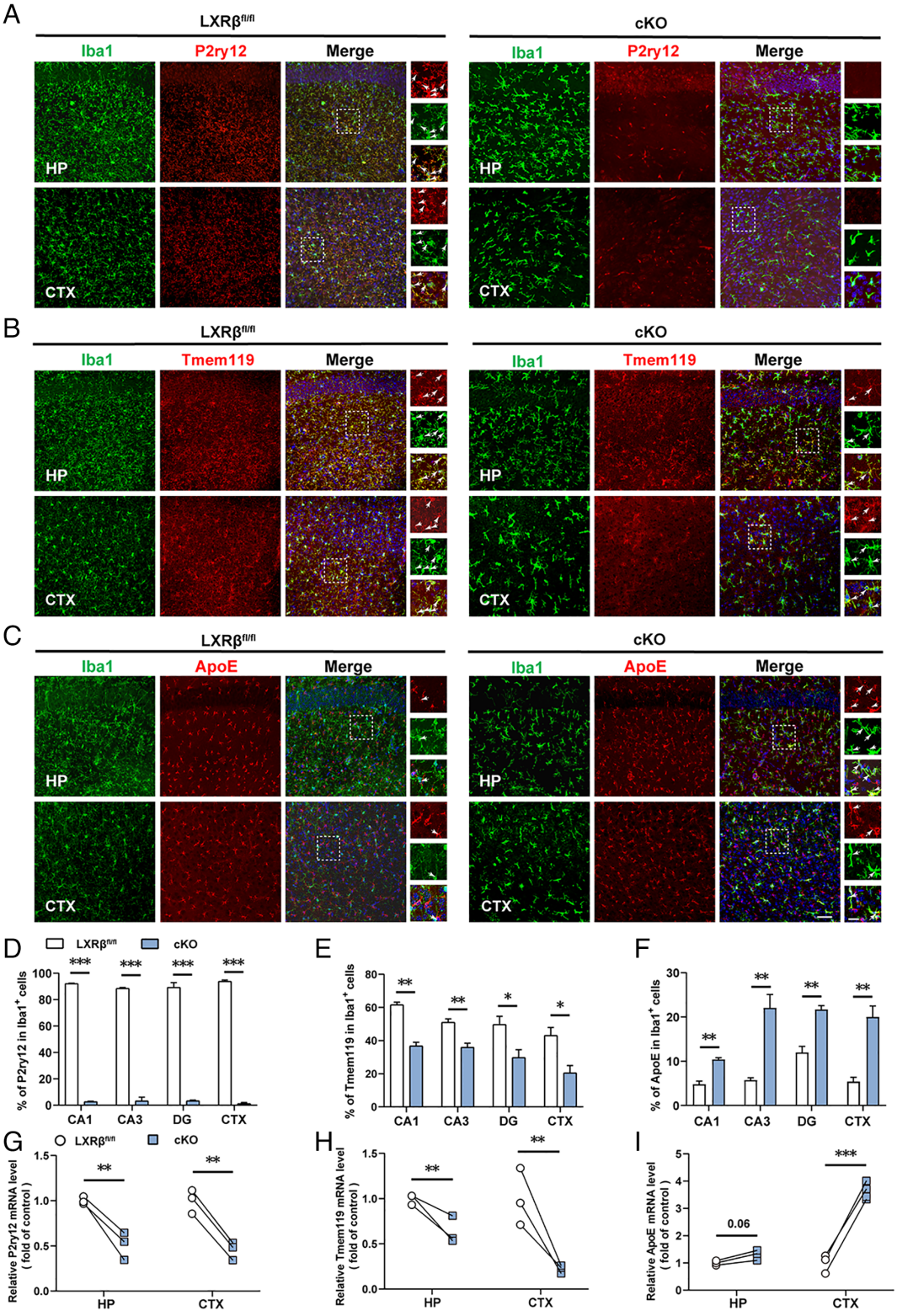

Fig. 4. Constitutive expression of microglial gene P2ry12, Tmem119, and ApoE upon LXRβ deletion in microglia at P14. (*A–C*) Representative images of coimmunofluorescence staining P2ry12 (*A*), Tmem119 (*B*), ApoE (*C*) with Iba1 from hippocampus and CTX of LXRβ$^{fl/fl}$ and cKO mice at P14. (Large view, Scale bar, 50 μm; short view, scale bar, 20 μm.) (*D–F*) Immunofluorescence analysis of ratios of Iba1/P2ry12/ (*D*), Iba1/Tmem119 (*E*), and Iba1/ApoE (*F*) in microglia (Iba1) in CA1, CA3, DG, and CTX of LXRβ$^{fl/fl}$ and cKO (N = 3 mice per group). (*G–I*) P2yr12 (*G*), Tmem119 (*H*), and ApoE (*I*) mRNA expressions were assessed by qRT-PCR in the CTX and hippocampus of LXRβ$^{fl/fl}$ and cKO mice at P14 (N = 3 to 4 mice per group). Data were shown as mean ± SEM. the student's *t* test. **P* < 0.05, ***P* < 0.01, ****P* < 0.001.

of microglial homeostasis genes in the hippocampus and cerebral cortex (Fig. 4 *G* and *H*). Notably, these microglial homeostasis differences were maintained in the microglia of the cKO at P30 (*SI Appendix*, Figs. S7 and S8). One gene whose expression was up-regulated in the hippocampus and cerebral cortex of cKO mice at P14 both at the protein (Fig. 4 *C* and *F*) and mRNA (Fig. 4*I*) level was ApoE. However, in contrast to P2ry12 and Tmem119, the increase in the ApoE expression seen in the P14 cKO mouse

was not seen at P30 (*SI Appendix*, Fig. S9). These data indicate that microglial LXRβ is essential for microglia homeostasis.

Specific Ablation of LXRβ in Microglia Increased Synapse Elimination. Specific ablation of LXRβ in microglia caused a decrease in expression of the postsynaptic marker, PSD95 levels in the hippocampus at both P14 (Fig. 5 *A* and *C*) and P30 (Fig. 5 *B* and *D*). However, loss of LXRβ did not affect synapsin and synaptophysin protein levels. We compared immunofluorescence staining for PSD95 and Iba1 in hippocampal CA1 sections from the cKO mouse and controls at P14 and P30 to analyze how much phagocytosis occurred. Loss of LXRβ in microglia led to decreased $PSD95^{+}$ puncta density in cKO mouse hippocampal CA1 at P14 (Fig. 5 *E* and *F*) and P30 (Fig. 5 *E* and *G*). Furthermore, quantitative analyses using Imaris software revealed an increase in PSD95 puncta engulfed in $Iba1^{+}$ cells at P14 (Fig. 5 *H* and *I*) and P30 (Fig. 5 *H* and *J*). These findings suggest that loss of LXRβ in microglia enhances synapse phagocytosis of microglia in the hippocampus.

We explored whether the enhanced synapse phagocytosis induced by microglial LXRβ deletion would be mirrored at the transcriptional level. Hierarchical clustering showed clear segregation of the DEGs in the hippocampus between the cKO and control mice (Fig. 5*K*). Analysis of the differences showed 110 up-regulated and 48 down-regulated genes (with >1.5-fold change and $P < 0.05$) (Fig. 5*L*). GO analysis showed that the top enriched clusters in the cellular component category contain the phagocytic-, endocytic-, and lysosomal- membrane vesicles (Fig. 5*M*). Gene set enrichment analysis (GSEA) showed several significantly important up-regulated pathways related to phagosomes in the cKO mice. These included "regulation of phagocytosis (*P*-value: 0; adj: 4.15e−04; NES: 2.115)" (Fig. 5*N*) and "phagocytic vesicle membrane (*P*-value: 0; adj: 9.79e−04; NES: 2.071)" (Fig. 5*O*). Furthermore, KEGG analysis showed that most DEGs were significantly enriched for the phagosome (Fig. 5*P*). The changes in the genes in the heatmap diagram analysis, including *H2-K1, H2-D1, H2-Q4, H2-Q6, Cybb, Mrc1, H2-Q7, Ctss, Thbs4, Clec7a* (Fig. 5*Q*), were validated by RT-qPCR (Fig. 5*R*).

Behavioral Studies in the Microglial-Specific KO Mice. Behavioral studies revealed that specific ablation of LXRβ in microglia impaired cognitive function in mice. At 2 to 3 mo of age after peripheral monocytes should have been replaced following tamoxifen injection (Fig. 6*A*), open-field (Fig. 6 *B*–*D*), light-dark box (Fig. 6*E*), and elevated plus-maze tests (Fig. 6*F*) showed that LXRβ microglial ablation did not affect locomotor or anxiety behaviors. As shown in Fig. 6*G*, the nesting score in the cKO mice was significantly lower than that in $LXR\beta^{fl/fl}$ mice, reflecting a decline in hippocampal-related cognitive ability. Two hippocampus-related memory tests were conducted further to validate this: the Y maze and novel object recognition (NOR) tests. Results showed that cKO mice performed poorly in both tests, with a lower rate of correct spontaneous alternation in the Y maze (Fig. 6 *H* and *I*) and reduced discrimination index in the NOR tests (Fig. 6 *J* and *K*). The Morris water maze (MWM) test evaluated hippocampus-dependent spatial learning and memory ability (Fig. 6*L*). During the learning phase, the cKO mice had a significantly longer escape latency on day 5 (day 5: $P < 0.05$) compared to control mice (Fig. 6*M*). The platform was removed on day 6, and a probe test showed that control mice spent more time in the target than in other quadrants, whereas no difference was detected in the spending time between the target and other quadrants in the cKO mice (Fig. 6*N*). No significant differences were observed in the number of times they crossed the platform ($P > 0.05$) (Fig. 6*O*) and swimming speed ($P > 0.05$) (Fig. 6*P*). In addition, we conducted cognitive flexibility and found that removing postnatal microglial LXRβ did not impact cognitive flexibility (Fig. 6 *Q*–*U*). The cKO mice continued to exhibit abnormal hippocampus-dependent cognitive dysfunction even at 10 mo of age (*SI Appendix*, Fig. S10).

When tamoxifen was administered at P30 to induce gene deletion after microglia had fully matured (*SI Appendix*, Fig. S11*A*), the mice displayed an intact motor function in the open-field test and no anxiety-like phenotype in an open field, elevated plus maze, and light–dark box tests (*SI Appendix*, Fig. S11 *A*–*E*). There was no effect on object recognition short-term memory in the NOR test (*SI Appendix*, Fig. S11*F*), working memory in the Y maze test (*SI Appendix*, Fig. S11*G*), or spatial learning and memory in the MWM test (*SI Appendix*, Fig. S11 *H*–*M*). Costaining with P2ry12 and Iba1 showed no difference between cKO and controls in the ratio of $P2ry12^{+}/Iba1^{+}$ cells in the hippocampus and cerebral cortex (*SI Appendix*, Fig. S11 *N*–*P*). Our results suggest that microglial homeostasis was not altered by loss of LXRβ in microglia after P30. These data demonstrate that LXRβ signaling is required for microglial maturation, but that removal of LXRβ signaling in microglia after microglia have matured has little effect on their homeostatic phenotype or cognitive functions.

Discussion

In this study, using microglial-specific LXRβ KO mice, we have demonstrated a critical role for LXRβ signaling in the maturation of microglia during the first 2 wk of postnatal life. The main effects on microglia were reduced number, hyper-activation, and enhanced synaptic engulfment, leading to cognitive defects that lasted in adult life. Removal of LXRβ from microglia in adult mice did not cause cognitive defects. Three stages of microglial development have been defined: an early phase in fetal life, a second phase spanning fetal day 14 to the first 2 wk of life, and an adult phase from 2 wk to adulthood. Each phase is regulated by the distinct conditions in the environment (36). Notably, our findings suggest that loss of LXRβ in microglia causes a developmental disorder, as deletion of LXRβ from immature microglia caused a marked phenotype, while deletion after maturation did not. A decline in microglia proliferation may be responsible for the decreased number of microglia observed in the cKO mice between P7 and P14. cKO mice have fewer $ki67^{+}$ microglia in the hippocampus and cortex from P7 to P14 than control mice. No difference was seen at P30 when both genotypes had a low proliferation rate.

Transcriptome analysis after RNA seq revealed that, in the cKO mice, transcription factors associated with microglial homeostasis were altered. These included Sall1, P2ry12, and Pu.1. Sall1 is required for early microglia to transition into a more mature status during development (37). It specifically regulates the expression of the purinergic receptor, P2ry12, expressed in ramified microglia processes (38). The transcription factor Pu.1, a master regulator of microglial gene expression, plays critical transcriptional regulatory roles in the transition between homeostatic to proinflammatory DAM (39). Transcriptomic profiling of microglia from cKO and control mice revealed significant enrichment in biological processes related to immune and inflammatory components in the cKO mice. Of note, LXRβ deletion in microglia promoted the up-regulation of activated and DAM genes, such as *ApoE, Axl, B2m, Cybb, Ctsz, Clec7a, Lyz2,* and *Tyrobp*, and the downregulation of homeostatic microglial genes *Cx3cr1, crybb1, slco2b1, Selplg, Csfr1, Fcrls, Tmem119,* and *Siglech.* When LXRβ is removed from microglia, there is an increase in mRNA expression of

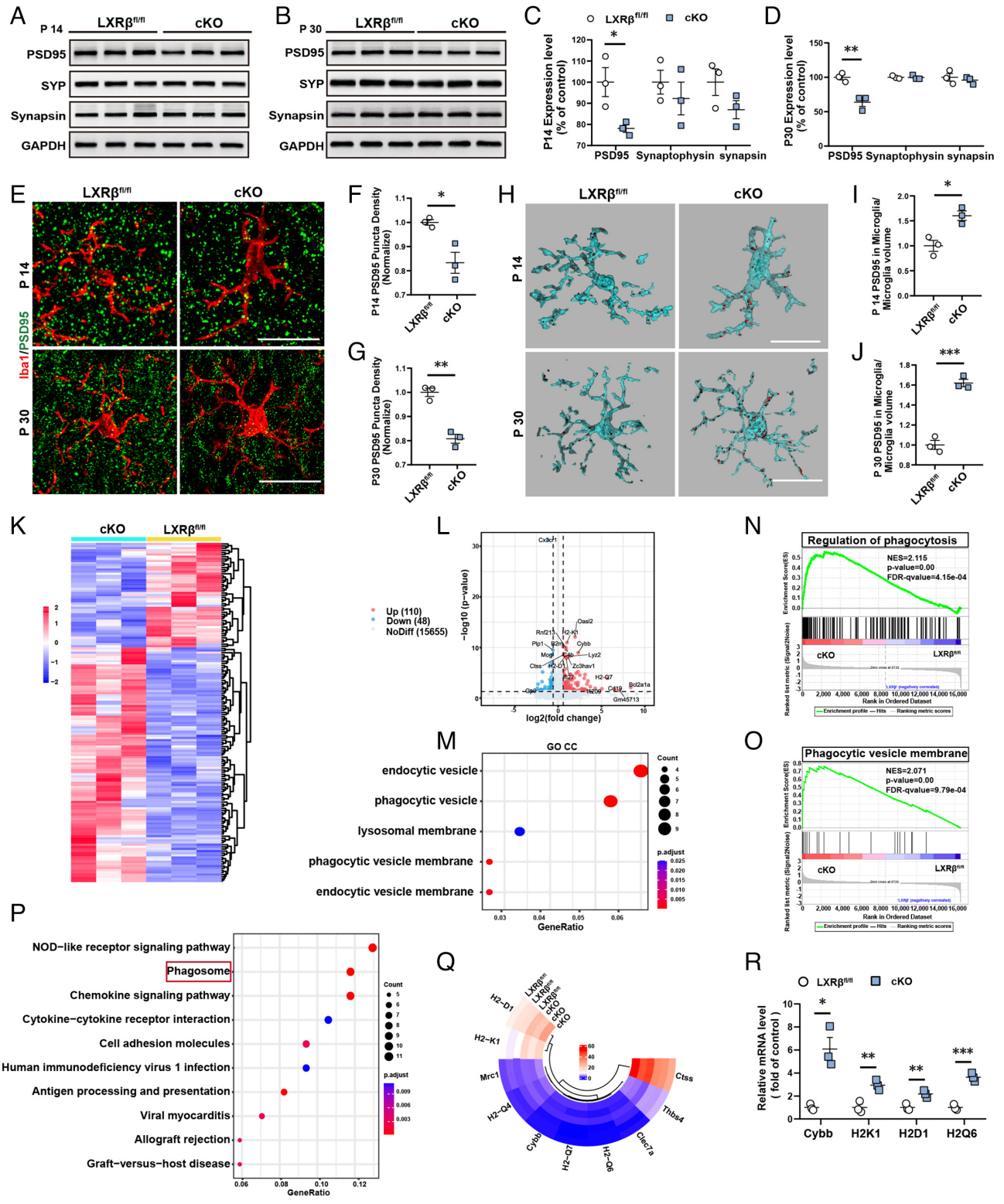

Fig. 5. LXRβ deficiency in microglia increases synapse elimination. (*A–D*) Representative western blottings and quantification of PSD95, synaptophysin (SYP), and synapsin in LXRβ$^{fl/fl}$ and cKO mouse hippocampus at P14 (*A* and *C*) and P30 (*B* and *D*) (N = 3 mice per group). (*E–G*) Representative confocal images of PSD95 colocalized with Iba1 in the hippocampal CA1 from LXRβ$^{fl/fl}$ mice and cKO mice at P14 and P30 (*E*). Quantitative analysis of PSD95 puncta at P14 (*F*) and P30 (*G*) (N = 3 mice per group). (Scale bar, 20 μm.) (*H–J*) Representative confocal images of 3D reconstruction of PSD95-positive puncta (green) engulfed in Iba1^{+} microglia (red) in the hippocampal CA1 from LXRβ$^{fl/fl}$ and cKO mice at P14 and P30 (*H*), Quantitative analysis of PSD95-positive puncta (green) engulfed in Iba1^{+} microglia at P14 (*I*), at P30 (*J*) (N = 3 mice per group). (Scale bar, 20 μm.) (*K*) Heatmap shows hierarchical clustering of up-regulated (red) and down-regulated (blue) genes in hippocampus tissue from LXRβ deficiency in microglia and LXRβ control analysis of RNA-Seq values (N = 3 mice per group). (*L*) A volcano plot displayed DEGs in the hippocampus of LXRβ$^{fl/fl}$ and cKO mice. (*M*) Functional enriched GO pathways in cellular components relate to phagocytic pathways. (*N* and *O*) GSEA revealed that deletion of LXRβ in microglia positively regulated the phagocytosis gene set, such as the regulation of phagocytosis (*N*) and phagocytic vesicle membrane (*O*). (*P*) Enriched top 10 KEGG pathways were selected for significant enrichment differences, where the phagosome signaling pathway has been highlighted in the red frame. (*Q*) The heatmap showed the 10 DEGs from the phagosome signaling pathway. Red represents relatively increased expression, and blue indicates relatively decreased expression. (*R*) qRT-PCR was performed to verify the genes regulated by "phagosome" pathways by RNA-seq (N = 3 mice per group). Data were shown as mean ± SEM. the student's *t* test. **P* < 0.05, ***P* < 0.01, ****P* < 0.001.

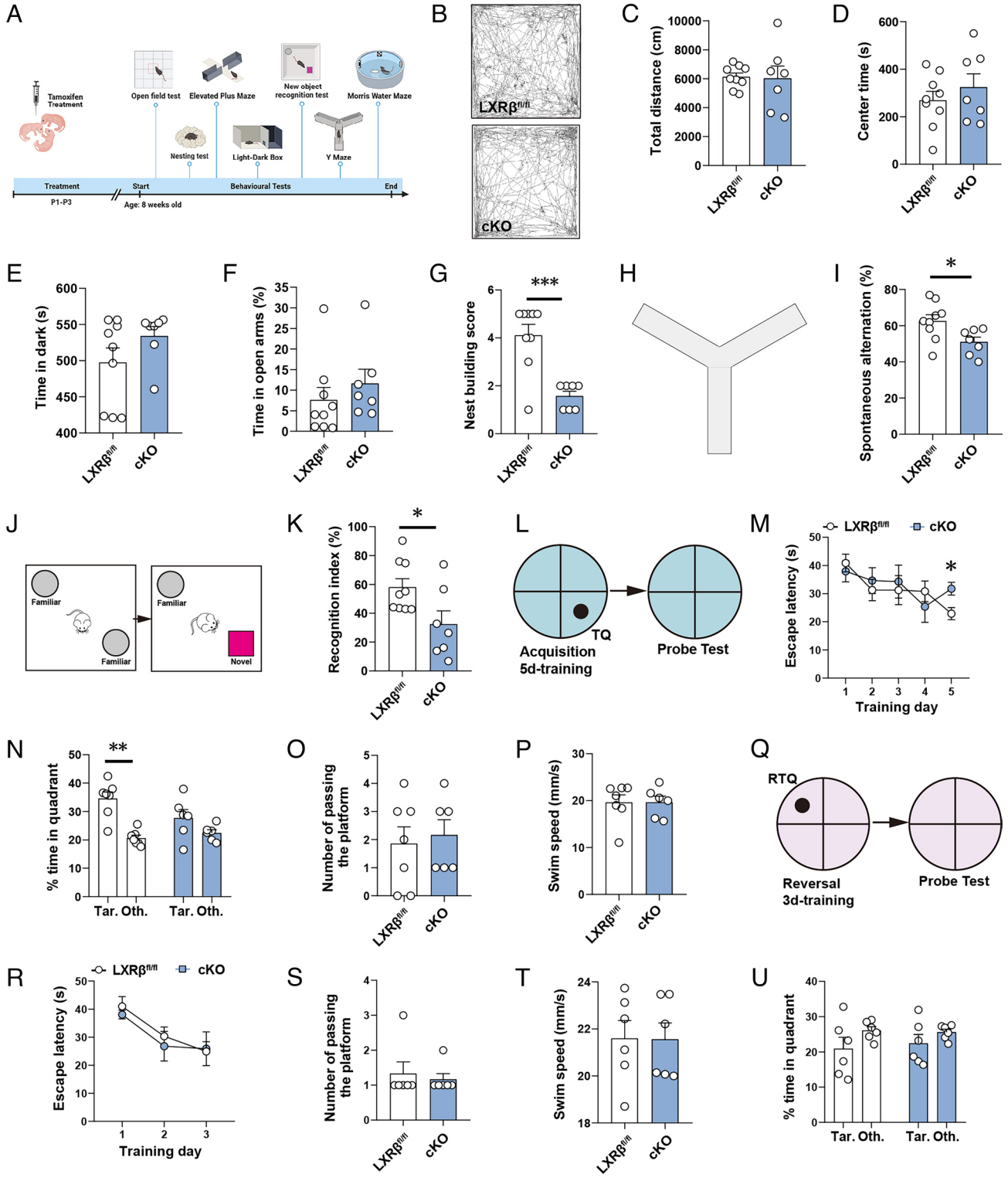

Fig. 6. Microglia-specific LXRβ ablation exhibits deficits in hippocampus-dependent learning and memory in mice. (*A*) Schematic diagram of behavioral experimental design. (*B*) A representative trace chart in the open field test between the two groups of mice. (*C* and *D*) The total distance (*C*) and center time (*D*) in the open field test. (*E*) The time spent in a dark box was assessed using a light–dark box test. (*F*) The elevated plus maze test assessed the percentage of time staying in the open arms. (*G*) The scores of nest building were evaluated in nesting building tests. (*H* and *I*) The experimental protocol of the Y maze test (*H*) and the performance in the Y maze test (*I*). (*J* and *K*) Experimental protocol of NOR test (*J*) and the performance in the NOR test (*K*). (*L*–*P*) Morris water maze test evaluated the escape latency to reach the platform during acquisition training. Schematic drawing of Morris water maze (*L*), representative time spent in the platform (*M*), the time in target quadrant and other quadrant (*N*), the number of crossing platforms (*O*), swim speed (*P*), and during probe trials of the Morris water maze test (TQ = Target quadrant). (*Q*–*U*) The reverse Morris water maze test was evaluated to escape latency and reach the opposite platform during acquisition training. Schematic drawing of reverse Morris water maze (*Q*), representative time spent in the platform (*R*), the number of crossing platforms (*S*), swim speed (*T*), and the time in the target quadrant and other quadrant during probe trials of the reverse Morris water maze test (*U*) (RTQ = Reversal Target quadrant). Data are presented as mean ± SEM. cKO mice (n = 6-7) and LXRβ$^{fl/fl}$ (n = 6-9) mice. *P < 0.05, **P < 0.01, ***P < 0.001.

microglial activation markers (CD68, MHC-II, and ApoE) and proinflammatory cytokines (TNF-α, IL-1β, and IL-6) in purified microglia. Immunofluorescence staining for P2ry12, Tmem119, and ApoE confirmed the involvement of LXRβ in microglia in both homeostasis- and inflammation-specific signal regulation. Since the ApoE pathway mediates a switch from homeostatic to neurodegenerative microglia (40), the findings suggest that constitutive LXRβ signaling is necessary to sustain homeostatic microglia-specific gene signatures and prevent a shift to an activated phenotype.

In the cKO mice between P14 and P30, there was enhanced synaptic engulfment and elimination of postsynaptic protein PSD95, resulting in synaptic loss and cognitive impairment. RNA-seq analysis confirmed up-regulated expression of transcripts related to phagosome formation, immune activation, and phagocytic pathways (*H2-K1, Cybb, Ctss, H2-D1, H2-Q7, H2-Q4, H2-Q6, Thbs4, Mrc1, and Clec7a*). In behavioral studies, we found that microglial LXRβ deletion in male mice in early postnatal life impaired object recognition, working memory, and spatial learning and memory. However, these defects did not occur when LXRβ was deleted in adult mice, and there were no changes in microglial morphology or homeostatic microglia. The role of LXRβ in microglia in gene regulation, as seen in mice, was confirmed in the microglial cell line, BV2. LXRβ-knockdown in these cells led to a significant decrease in Sall1 and P2ry12 mRNA expression. Expression of P2ry12 was restored by Sall1 overexpression.

Several strengths and limitations of this study can inform future research. Evidence has shown the heterogeneity of microglia-like clusters in early postnatal microglia (41). This is an essential consideration in understanding LXRβ in typical microglia-like clusters. Additionally, proliferative region-associated microglia (PAMs) have been found in developing white-matter areas in the postnatal brain (42), and it has been confirmed that PAMs share a characteristic gene signature with DAM (43). Further studies are needed to examine the role of LXRβ in PAMs. The deletion of LXRβ from immature microglia resulted in a developmental disorder, prompting new inquiries into how specific neurons shape circuits and contribute to plasticity. Additional studies should assess the circuit function associated with the phagocytic behavior induced by the deletion of LXRβ in microglia.

In summary, these findings suggest that endogenous LXRβ activity in microglia is essential for proper homeostasis and maintaining the expression of canonical microglial markers. The timing of microglia loss of LXRβ was critical for microglial maturation. A reduction in LXRβ signaling during early postnatal development results in disturbance of microglial properties, which pushes microglia from a state of equilibrium into an activated state with DAM-gene profiles, ultimately resulting in cognitive dysfunction later in life.

Methods and Materials

Cell-specific LXRβ knockout mice were generated using the Cre/loxP system. The $LXR\beta^{fl/fl}$ mice were from Ozgene Pty, Ltd. (Bentley DC, Australia), referred to as control mice in this study, and the $Cx3cr1^{CreER}$ mice (stock no. 021160) were from Jackson Laboratory to produce $Cx3cr1^{CreER}$. $LXR\beta^{fl/fl}$ mice, referred to as cKO mice in this study. Rosa26-LSL-tdTomato reporter (Rosa-tdTomato) from Shanghai Model Organisms Center, Inc. China crossed to the $Cx3cr1^{CreER}$ mice to generate $Cx3cr1^{CreER}$:Rosa26 mice. Male mice have been used throughout the study. To induce CreER activity in $Cx3cr1^{CreER}$:$LXR\beta^{fl/fl}$, tamoxifen (T5648, Sigma) dissolved in corn oil (Sigma, C8267) was given intraperitoneally (IP) starting at P1 (50 μg) once a day for three consecutive days (44) or at P30 with tamoxifen daily at 100 mg/kg for five consecutive days as described previously (45). Animals were maintained in a 12:12 h light:dark cycle with free access to food and water. All efforts were taken to minimize the pain or discomfort of the mice during the study. The Third Military Medical University Institutional Animal Care and Use Committee approved all experimental procedures.

Immunohistochemistry (IHC), Three-dimensional reconstruction of microglia, Isolation of microglia for flow cytometry and Fluorescence activated microglial cell sorting (FACS), Behavioral analyses, Western blotting, qRT-PCR, Cell culture and Cell transfection, RNA isolation and sequencing, and Statistical analysis were conducted according to published protocols. Information for detailed experimental procedures, the sequences of primers, and analyses can be found in the *SI Appendix*.

Data, Materials, and Software Availability. The raw sequencing data generated in this study have been deposited in the NCBI Sequence Read Archive (SRA) under the accession number PRJNA1111295. All data is publicly accessible and can be retrieved via the following link: https://www.ncbi.nlm.nih.gov/sra/?term=PRJNA1111295 (46). All other data are included in the manuscript and/or *SI Appendix*.

ACKNOWLEDGMENTS. This study was supported by National Key R&D Program of China (2021YFA1101203), the National Nature Science Foundation of China (No. 32471027, No. 82101245), the Natural Science Foundation Project of Chongqing (CSTB2023NSCQBHX0076), and the Swedish Research Council and a grant from the Robert A. Welch Foundation (E-0004, J.-Å.G.).

Author affiliations: [a]Department of Military Cognitive Psychology, School of Psychology, Third Military Medical University (Army Medical University), Chongqing 400038, China; [b]Southwest Eye Hospital, Southwest Hospital, Third Military Medical University (Army Medical University), Chongqing 400038, China; [c]Center for Innovative Medicine, Department of Biosciences and Nutrition, Karolinska Institute, Stockholm 14186, Sweden; and [d]Center for Nuclear Receptors and Cell Signaling, University of Houston, Houston, TX 77204

1. D. P. Schafer, E. K. Lehrman, B. Stevens, The "quad-partite" synapse: Microglia-synapse interactions in the developing and mature CNS. *Glia* **61**, 24–36 (2013).
2. E. Bar, B. Barak, Microglia roles in synaptic plasticity and myelination in homeostatic conditions and neurodevelopmental disorders. *Glia* **67**, 2125–2141 (2019).
3. T. Balzano *et al.*, Chronic hyperammonemia induces peripheral inflammation that leads to cognitive impairment in rats: Reversed by anti-TNF-alpha treatment. *J. Hepatol.* **73**, 582–592 (2020).
4. S. Talley *et al.*, DSS-induced inflammation in the colon drives a proinflammatory signature in the brain that is ameliorated by prophylactic treatment with the S100A9 inhibitor paquinimod. *J. Neuroinflammation* **18**, 263 (2021).
5. N. Piehl *et al.*, Cerebrospinal fluid immune dysregulation during healthy brain aging and cognitive impairment. *Cell* **185**, 5028–5039 (2022).
6. K. Krukowski *et al.*, Novel microglia-mediated mechanisms underlying synaptic loss and cognitive impairment after traumatic brain injury. *Brain Behav. Immun.* **98**, 122–135 (2021).
7. S. Schilling *et al.*, TLR2- and TLR3-activated microglia induce different levels of neuronal network dysfunction in a context-dependent manner. *Brain Behav. Immun.* **96**, 80–91 (2021).
8. D. Zhang *et al.*, Microglial activation contributes to cognitive impairments in rotenone-induced mouse Parkinson's disease model. *J. Neuroinflammation* **18**, 4 (2021).
9. Y. Yasumoto *et al.*, Ucp2-dependent microglia-neuronal coupling controls ventral hippocampal circuit function and anxiety-like behavior. *Mol. Psychiatry* **26**, 2740–2752 (2021).
10. G. Piccioni, D. Mango, A. Saidi, M. Corbo, R. Nistico, Targeting microglia-synapse interactions in Alzheimer's disease. *Int. J. Mol. Sci.* **22**, 2342 (2021).
11. C. Wang *et al.*, Microglia mediate forgetting via complement-dependent synaptic elimination. *Science* **367**, 688–694 (2020).
12. X. Ding *et al.*, Loss of microglial SIRPα promotes synaptic pruning in preclinical models of neurodegeneration. *Nat. Commun.* **12**, 2030 (2021).
13. T. Masuda, R. Sankowski, O. Staszewski, M. Prinz, Microglia heterogeneity in the single-cell era. *Cell Rep.* **30**, 1271–1281 (2020).
14. Y. J. Xu, N. P. B. Au, C. H. E. Ma, Functional and phenotypic diversity of microglia: Implication for microglia-based therapies for Alzheimer's disease. *Front. Aging Neurosci.* **14**, 896852 (2022).
15. T. Jakobsson, E. Treuter, J. A. Gustafsson, K. R. Steffensen, Liver X receptor biology and pharmacology: New pathways, challenges and opportunities. *Trends Pharmacol. Sci.* **33**, 394–404 (2012).
16. K. D. Whitney *et al.*, Regulation of cholesterol homeostasis by the liver X receptors in the central nervous system. *Mol. Endocrinol.* **16**, 1378–1385 (2002).
17. Y. Cai *et al.*, Liver X receptor beta regulates the development of the dentate gyrus and autistic-like behavior in the mouse. *Proc. Natl. Acad. Sci. U.S.A.* **115**, E2725–E2733 (2018).

18. Y. Dai *et al.*, Liver X receptors regulate cerebrospinal fluid production. *Mol. Psychiatry* **21**, 844–856 (2016).
19. X. Fan, H. J. Kim, D. Bouton, M. Warner, J. A. Gustafsson, Expression of liver X receptor beta is essential for formation of superficial cortical layers and migration of later-born neurons. *Proc. Natl. Acad. Sci. U.S.A.* **105**, 13445–13450 (2008).
20. H. J. Kim *et al.*, Liver X receptor beta (LXRbeta): A link between beta-sitosterol and amyotrophic lateral sclerosis-Parkinson's dementia. *Proc. Natl. Acad. Sci. U.S.A.* **105**, 2094–2099 (2008).
21. S. Andersson, N. Gustafsson, M. Warner, J. A. Gustafsson, Inactivation of liver X receptor beta leads to adult-onset motor neuron degeneration in male mice. *Proc. Natl. Acad. Sci. U.S.A.* 102, 3857–3862 (2005).
22. X. Li *et al.*, Loss of liver X receptor beta in astrocytes leads to anxiety-like behaviors via regulating synaptic transmission in the medial prefrontal cortex in mice. *Mol. Psychiatry* **26**, 6380–6393 (2021).
23. Y. Dai, X. Tan, W. Wu, M. Warner, J. Å. Gustafsson, Liver X receptor β protects dopaminergic neurons in a mouse model of Parkinson disease. *Proc. Natl. Acad. Sci. U.S.A.* **109**, 13112–13117 (2012).
24. X. Bao *et al.*, Liver X receptor β is involved in formalin-induced spontaneous pain. *Mol. Neurobiol.* **54**, 1467–1481 (2017).
25. C. X. Zhang-Gandhi, P. D. Drew, Liver X receptor and retinoid X receptor agonists inhibit inflammatory responses of microglia and astrocytes. *J. Neuroimmunol.* **183**, 50–59 (2007).
26. J. R. Secor McVoy *et al.*, Liver X receptor-dependent inhibition of microglial nitric oxide synthase 2. *J. Neuroinflammation* **12**, 27 (2015).
27. J. F. J. Bogie *et al.*, Liver X receptor beta deficiency attenuates autoimmune-associated neuroinflammation in a T cell-dependent manner. *J. Autoimmun.* **124**, 102723 (2021).
28. K. Endo-Umeda *et al.*, Myeloid LXR (liver X receptor) deficiency induces inflammatory gene expression in foamy macrophages and accelerates atherosclerosis. *Arterioscler. Thromb. Vasc. Biol.* **42**, 719–731 (2022).
29. M. T. Bilotta, S. Petillo, A. Santoni, M. Cippitelli, Liver X receptors: Regulators of cholesterol metabolism, inflammation, autoimmunity, and cancer. *Front. Immunol.* **11**, 584303 (2020).
30. X. Xu, X. Xiao, Y. Yan, T. Zhang, Activation of liver X receptors prevents emotional and cognitive dysfunction by suppressing microglial M1-polarization and restoring synaptic plasticity in the hippocampus of mice. *Brain Behav. Immun.* **94**, 111–124 (2021).
31. T. Gao *et al.*, Transcriptional regulation of homeostatic and disease-associated-microglial genes by IRF1, LXRbeta, and CEBPalpha. *Glia* **67**, 1958–1975 (2019).
32. K. Kierdorf *et al.*, Microglia emerge from erythromyeloid precursors via Pu.1- and Irf8-dependent pathways. *Nat. Neurosci.* **16**, 273–280 (2013).
33. A. Reifschneider *et al.*, Loss of TREM2 rescues hyperactivation of microglia, but not lysosomal deficits and neurotoxicity in models of progranulin deficiency. *EMBO J.* **41**, e109108 (2022).
34. M. L. Bennett *et al.*, New tools for studying microglia in the mouse and human CNS. *Proc. Natl. Acad. Sci. U.S.A.* **113**, E1738–E1746 (2016).
35. K. Saeki *et al.*, IRF8 defines the epigenetic landscape in postnatal microglia, thereby directing their transcriptome programs. *Nat. Immunol.* **25**, 1928–1942 (2024).
36. O. Matcovitch-Natan *et al.*, Microglia development follows a stepwise program to regulate brain homeostasis. *Science* **353**, aad8670 (2016).
37. A. Buttgereit *et al.*, Sall1 is a transcriptional regulator defining microglia identity and function. *Nat. Immunol.* **17**, 1397–1406 (2016).
38. P. Banerjee *et al.*, Generation of pure monocultures of human microglia-like cells from induced pluripotent stem cells. *Stem Cell Res.* **49**, 102046 (2020).
39. H. Yeh, T. Ikezu, Transcriptional and epigenetic regulation of microglia in health and disease. *Trends Mol. Med.* **25**, 96–111 (2019).
40. S. Krasemann *et al.*, The TREM2-APOE pathway drives the transcriptional phenotype of dysfunctional microglia in neurodegenerative diseases. *Immunity* **47**, 566–581 (2017).
41. R. C. Paolicelli *et al.*, Microglia states and nomenclature: A field at its crossroads. *Neuron* **110**, 3458–3483 (2022).
42. K. M. Barclay *et al.*, An inducible genetic tool to track and manipulate specific microglial states reveals their plasticity and roles in remyelination. *Immunity* **57**, 1394–1412 (2024).
43. Q. Li *et al.*, Developmental heterogeneity of microglia and brain myeloid cells revealed by deep single-cell RNA sequencing. *Neuron* **101**, 207–223 (2019).
44. M. E. Pitulescu, I. Schmidt, R. Benedito, R. H. Adams, Inducible gene targeting in the neonatal vasculature and analysis of retinal angiogenesis in mice. *Nat. Protoc.* **5**, 1518–1534 (2010).
45. X. Zhao *et al.*, Noninflammatory changes of microglia are sufficient to cause epilepsy. *Cell Rep.* **22**, 2080–2093 (2018).
46. K. Lv *et al.*, transcriptomics of microglia and the hippocampus of p14mouse. Sequence Read Archive. https://www.ncbi.nlm.nih.gov/bioproject?term=PRJNA1111295. Deposited 14 May 2024.